

# PGMAN: An Unsupervised Generative Multi-adversarial Network for Pan-sharpening

Huanyu Zhou, Qingjie Liu, *Member, IEEE*, Yunhong Wang, *Fellow, IEEE*

**Abstract**—Pan-sharpening aims at fusing a low-resolution (LR) multi-spectral (MS) image and a high-resolution (HR) panchromatic (PAN) image acquired by a satellite to generate an HR MS image. Many deep learning based methods have been developed in the past few years. However, since there are no intended HR MS images as references for learning, almost all of the existing methods down-sample the MS and PAN images and regard the original MS images as targets to form a supervised setting for training. These methods may perform well on the down-scaled images, however, they generalize poorly to the full-resolution images. To conquer this problem, we design an unsupervised framework that is able to learn directly from the full-resolution images without any preprocessing. The model is built based on a novel generative multi-adversarial network. We use a two-stream generator to extract the modality-specific features from the PAN and MS images, respectively, and develop a dual-discriminator to preserve the spectral and spatial information of the inputs when performing fusion. Furthermore, a novel loss function is introduced to facilitate training under the unsupervised setting. Experiments and comparisons with other state-of-the-art methods on GaoFen-2 and QuickBird images demonstrate that the proposed method can obtain much better fusion results on the full-resolution images. Code is available<sup>1</sup>.

**Index Terms**—pan-sharpening, image fusion, unsupervised learning, generative adversarial network

## I. INTRODUCTION

**D**ue to physical constraints, most satellites such as QuickBird, GaoFen-1, 2, WorldView I, II only offer a pair of modalities at the same time: multi-spectral (MS) images at a low spatial resolution and panchromatic (PAN) images at a high spatial resolution. In many practical applications, it is desired to use high-resolution (HR) MS images. Pan-sharpening, which combines the strengths of a MS image with a PAN image to generate a HR MS image, provides a good solution to this.

Over the past few decades, numerous methods have been proposed for pan-sharpening. To distinguish those from the recently proposed deep learning models we called them traditional pan-sharpening methods, including Brovey [1], HPF [2] and LMVM [3], etc. Traditional methods are widely used in practice, however, their ability to solve highly nonlinear mapping is limited and thus often suffer from spatial or spectral distortions. Recently, deep learning techniques have made great advancements in various computer vision tasks, ranging from low-level image processing to high-level image understanding. Inspired by this, many deep learning models have been developed for pan-sharpening. PNN [4] introduces

SRCNN [5] to pan-sharpening and designs a fusion network which is also a 3-layered CNN. PanNet [6] uses skip-connections [7] to build deeper networks and trains the model on the high-frequency domain to learn the residuals between the up-sampled LR MS images and the desired HR MS images. TFNet [8] builds a two-stream fusion network to perform pan-sharpening, in which features of PAN and MS images are extracted separately using two distinct sub-networks. PSGAN [9] improves the TFNet [8] by using generative adversarial training [10].

These deep learning methods for pan-sharpening have achieved satisfactory performances. However, they cannot be optimized without supervised images and hence are hard to obtain optimal results on the full-resolution images. To be specific, the existing works require ideal HR MS images which do not exist to train networks. To conquer this problem, they down-sample PAN and MS images and take the original MS image as targets to form training samples. In the testing stage, evaluations are also conducted on the down-sampled images. These methods may have good performances in the down-sampled image domain, however, they generalize poorly to the original full-scale images, which makes them lack practicality.

To overcome this drawback, we propose an unsupervised generative multi-adversarial network, termed PGMAN. PGMAN focuses on unsupervised learning and is trained on the original data without down-sampling or any other preprocessing steps to make full use of original spatial and spectral information. Our method is inspired by CycleGAN [11]. We use a two-stream generator to extract modality-specific features from PAN and MS images, respectively. Since we do not have target images to calculate losses, the only way for us to verify the quality of the generated images is the consistency property between the pan-sharpened images and the PAN and MS images, i.e. the degraded versions of the HR MS images, both spectral and spatial degradations, should be as close as possible to the PAN and MS images. To realize this, we build two discriminators, down-sample and gray the fusion result for the two discriminators to distinguish them from the original inputs. Furthermore, inspired by the non-reference metric *QNR* [12], we introduce a novel loss function to boost the quality of the pan-sharpened images. Our major contributions can be summarized as follows:

- We design an unsupervised generative multi-adversarial network for pan-sharpening, termed PGMAN, which can be trained on the full-resolution PAN and MS images to take advantage of rich spatial and spectral information of the original data.
- For the purpose of being consistent with the original PAN

<sup>1</sup><https://github.com/zhysora/PGMAN>

and MS images, we design a dual-discriminator architecture to preserve the spatial and spectral information.

- Inspired by the *QNR* metric, We introduce a novel loss to optimize the network under the unsupervised learning framework.
- We conduct extensive experiments on Gaofen-2 and QuickBird images and compare them with state-of-the-art methods. Experimental results demonstrate that the proposed method can achieve the best results on the full-resolution images, which clearly show its practical value.

## II. RELATED WORK

Deep learning techniques have achieved great success in diverse computer vision tasks, inspiring us to design deep learning models for the pan-sharpening problem. Observing that pan-sharpening and single image super-resolution share a similar spirit and motivated by [5], Masi et al. [4] proposes a three-layered convolutional neural network (CNN) based pan-sharpening method. Following this work, increasing research efforts have been devoted to developing deep learning based pan-sharpening. The first attempt at applying the residual network is PanNet [6]. They learn to predict high-frequency details of the image rather than the image itself. In this way, both spatial and spectral information could be preserved well.

Generative adversarial networks (GANs), proposed by Goodfellow et al. [10], have achieved attractive performance in various image generation tasks. The main idea of GANs is to train a generator with a discriminator, adversarially. The generator learns to output realistic images to cheat the discriminator while the discriminator learns to distinguish the generated images from real ones. However, the difficulty of stable training of GANs remains a problem. WGAN [13] leverages the Wasserstein distance as the objective function and uses weight clipping to stabilize the training process. WGAN-GP [14] penalizes norms of gradients of discriminators with respect to its input rather than uses weight clipping. To speed up convergence and ease training we choose WGAN-GP as the basic GAN to build our model.

Recently, researchers do not limit GANs to one generator and one discriminator and try to design multiple generators and discriminators for difficult tasks. GMAN [15] extends GANs to multiple discriminators and endows them with two roles: formidable adversaries and forgiving teachers. One is stronger discriminator while another is weaker. CycleGAN [11] designs two pairs of generators and discriminators and proposes a cycle consistency loss to reduce the space of possible mapping functions. Considering the domain-specific knowledge of panning-sharpening, we design two discriminators to train against one generator for spectral and spatial preservation.

### III. METHOD

## A. Network Architecture

1) *Generator*: We design the generator based on the architecture of TFNet [8] and make following modifications on it for further improving the quality of the pan-sharpened images. Firstly, inspired by PanNet [6], the generator is trained in the high-pass domain and the output of it is added to the

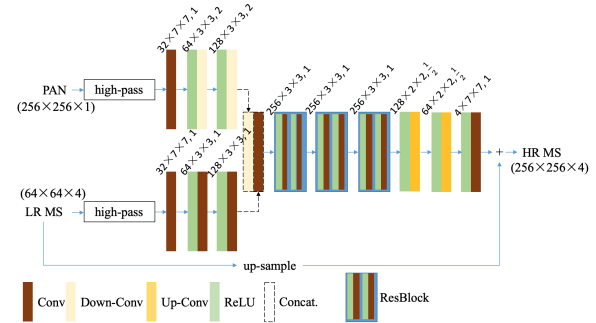


Fig. 1. The architecture of our generator.

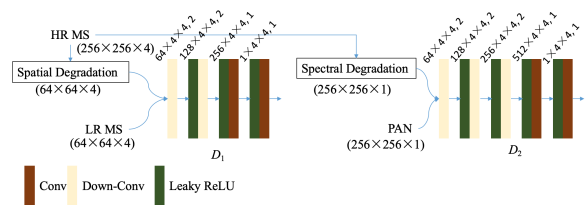


Fig. 2. The architecture of our discriminators.

up-sampled LR MS image for better spectral preservation. Secondly, considering that the input pair PAN and MS are with different sizes, we build two independent feature extraction (FE) sub-networks. The PAN FE sub-network has two stride-2 convolutions for down-sampling, while the MS FE sub-network has two stride-1 convolutions to maintain the feature map resolution without down-sampling. We concatenate feature maps produced by these two sub-networks and append three residual blocks [7] to achieve fusion. Finally, two successive fractionally-strided convolutions that both are with a stride of  $\frac{1}{2}$  are applied to up-sample the feature maps to meet the size of the desired HR MS. The outputs are high-frequency parts of the pan-sharpened MS images. We add them to the up-sampled LR MS images to obtain the final results. Fig. 1 shows the architecture of our generator.

2) *Discriminators*: We use two discriminators for verifying the consistency in pan-sharpening process. Firstly, we downsample the fused images to the same spatial resolution as the LR MS images and then apply the discriminator-1  $D_1$  to enforce them to have the same spectral information. Secondly, the discriminator-2  $D_2$  is applied to match the spatial structures of the intensity images of the fused images to that of the PAN images. We use discriminators similar to the one used in [16]. Since the input LR MS and PAN are with different image sizes and channels, the two discriminators have distinct architectures as shown in Fig. 2.  $D_2$  has one more convolution layer to downsample the feature maps because PAN images have a larger image size. As suggested by WGAN-GP [14], we remove the last activation function and batch normalization layers in our discriminators.

### B. Loss Function

1) *QNR Loss*: Supervised learning-based methods usually employ  $L_1$  or  $L_2$  loss to train the networks. However, under

unsupervised setting, there are no ideal images to be compared with. In this work, we attempt to devise an alternative solution that can quantify the quality of the fusion result with reference to the inputs rather than the ground truth. The intuition behind this is that there must be some consistencies across scales, which means there is a measure that we can obtain in low-resolution MS images and it still holds when applying it to the HR pan-sharpened MS images. This assumption has been studied by [17] and is the reason why we can generalize models trained under Wald's protocol to the original image space, i.e. we believe that the performances of models are invariant to scale changes.

Recall that, in the pan-sharpening paradigm, the inter-relationships between any couple of spectral bands of MS images should be unchanged after fusion, otherwise the pan-sharpened MS images may have spectral distortions. Furthermore, the inter-relationships between each band of the MS and the same sized PAN image should be preserved across scales. To describe this, quantitatively, we introduce QNR [12] and construct a non-GT loss on top of it, which defined as follows:

$$\mathcal{L}_{QNR} = 1 - QNR \quad (1)$$

This loss function enables us to measure the qualities of the fused images from input PAN and MS images without ground truth HR MS images.

2) *Adversarial Loss*: We design two discriminators,  $D_1$  for spectral preservation and  $D_2$  for spatial preservation. The loss function of the generator  $G$  takes the form of:

$$\begin{aligned} \mathcal{L}_G = \frac{1}{N} \sum_{n=1}^N -\alpha D_1(\tilde{P}^{(n)}) - \beta D_2(\hat{P}^{(n)}) \\ + \mathcal{L}_{QNR}(P^{(n)}, X^{(n)}, Y^{(n)}) \end{aligned} \quad (2)$$

where  $N$  is the number of samples.  $P$ ,  $X$ ,  $Y$  are pan-sharpened MS, PAN and LR MS images, respectively.  $\tilde{P}$  and  $\hat{P}$  stand for the spatially and spectrally degraded  $P$ .  $\alpha$  and  $\beta$  are hyper-parameters.

To stabilize the training, we employ WGAN-GP [14] as a basic model, i.e., using Wasserstein distance [13] and applying gradient penalty [14] to discriminators. The loss functions of  $D_1$  and  $D_2$  are formulated as follows:

$$\begin{aligned} \mathcal{L}_{D_1} = \frac{1}{N} \sum_{n=1}^N -D_1(X^{(n)}) + D_1(\tilde{P}^{(n)}) \\ + \lambda GP(D_1, X^{(n)}, \tilde{P}^{(n)}) \end{aligned} \quad (3)$$

$$\begin{aligned} \mathcal{L}_{D_2} = \frac{1}{N} \sum_{n=1}^N -D_2(Y^{(n)}) + D_2(\hat{P}^{(n)}) \\ + \lambda GP(D_2, Y^{(n)}, \hat{P}^{(n)}) \end{aligned} \quad (4)$$

where  $GP$  is the gradient penalty for discriminators and  $\lambda$  is a hyper-parameter.

### C. Training Details

Our method is implemented in PyTorch [18] and trained on a single NVIDIA Titan 1080Ti GPU. The batch size and

learning rate are set as 8 and 1e-4, respectively. The hyper-parameters in Eqs. 2, 3 and 4 are set as  $\alpha = 2e - 4$ ,  $\beta = 1e - 4$ , and  $\lambda = 100$ . Adam optimizer [19] is used to train the model for 20 epochs with fixed hyper-parameters  $\beta_1 = 0$  and  $\beta_2 = 0.9$ . In addition, we process the images at the raw bit depth in both training and testing.

## IV. EXPERIMENTS AND RESULTS

### A. Datasets and Metrics

We conduct extensive experiments on two datasets with images collected from GaoFen-2 and QuickBird satellites. For comparison with other methods, we report results under both Wald's protocol [17] and full-scale setting. Under full-scale setting, models are trained in an unsupervised manner. We use six reference-based indexes, including SAM [20], sCC [21], ERGAS [22], Q<sub>4</sub> [23], SSIM [24], and PSNR to evaluate the performances of the proposed and the comparison methods. Since there are no reference images under full-scale setting, we use QNR [12] to quantify the quality of the pan-sharpened images.

### B. Comparison with State-of-the-arts

Six methods including three traditional methods and three deep learning based methods are employed for comparison.

**Traditional methods** include Brovey [1], HPF [2] and LMVM [3]. These methods can be tested without training and can be applied to both down-sampled and full-scale images.

**Deep learning-based methods** are PNN [4], PanNet [6] and PSGAN [9]. These methods are state-of-the-art supervised deep learning based pan-sharpening methods. They are trained and tested under Wald's protocol. We generalize them to the full-scale images to obtain pan-sharpened MS images and compute QNR indicator for comparison.

**Our method** can be trained and tested under both settings, so we report quantitative results on both down-sampled and full-scale pan-sharpened images. Note that no ground truth images are used in our method during training.

### C. Quantitative Results

Table I and Table II show the quantitative assessments on GaoFen-2 and QuickBird test sets, respectively. From these two tables, we can see that under Wald's protocol deep learning methods achieve very good performances on these two datasets. PSGAN performs the best on the GaoFen-2 images and PanNet is the best approach on the QuickBird images, showing the powerful feature representation ability of deep learning models. Our method, i.e. PGMAN(W) also demonstrates good results on the two datasets. As can be seen, it obtains competitive performances to traditional methods and sometimes even better. Considering that there are no ground truth images are used, the results are quite promising.

When training on full-scale images, our method has potential that can further boost the performances. As can be observed from Tables I and II, PGMAN(F) shows improved quantitative indicators than PGMAN(W) and surpasses PNN, Brovey, and HPF in terms of almost all reference metrics

TABLE I

QUANTITY RESULTS ON GAOFEN-2 DATASETS. PGMAN (W) MEANS OUR METHOD IS TRAINED UNDER WALD'S PROTOCOL THAT IS ON DOWN-SAMPLED MS AND PAN IMAGES WHILE PGMAN (F) INDICATES OUR METHOD TRAINED ON FULL-SCALE IMAGES. NOTE THAT NO GROUND TRUTH IMAGES ARE USED UNDER BOTH SETTINGS.

Model	SAM ↓	sCC ↑	ERGAS ↓	Q4 ↑	SSIM ↑	PSNR ↑		QNR ↑
Brovey [1]	1.7377±0.0422	0.8946±0.0004	3.4325±0.1022	0.8415±0.0007	0.8293±0.0003	31.7863±0.7937		0.9265±0.0017
HPF [2]	2.0829±0.0535	0.9454±0.0001	4.1046±0.2004	0.8682±0.0006	0.8097±0.0004	30.8446±0.9487		0.9618±0.0003
LMVM [3]	1.8629±0.0462	0.9360±0.0002	2.7147±0.1086	0.9213±0.0003	0.8861±0.0002	34.4117±0.9189		0.8979±0.0012
PNN [4]	1.3513±0.0146	0.9650±0.0001	1.5140±0.0391	0.9770±0.0000	0.9636±0.0000	39.2457±1.0152		0.9634±0.0003
PanNet [6]	1.1209±0.0142	0.9713±0.0000	1.3399±0.0308	0.9814±0.0000	0.9696±0.0000	40.3543±1.0536		0.8791±0.0018
PSGAN [9]	1.0116±0.0095	0.9776±0.0000	1.1736±0.0195	0.9858±0.0000	0.9759±0.0000	41.5100±0.8843		0.8841±0.0016
PGMAN (W)	2.4507±0.0975	0.9115±0.0005	3.5348±0.2588	0.8923±0.0006	0.8478±0.0005	32.4329±1.1789		0.9514±0.0003
PGMAN (F)	2.0763±0.0314	0.9342±0.0002	2.5761±0.0707	0.9385±0.0001	0.9151±0.0001	34.8360±0.7312		0.9874±0.0000

TABLE II  
QUANTITY RESULTS ON QUICKBIRD DATASETS.

Model	SAM ↓	sCC ↑	ERGAS ↓	Q4 ↑	SSIM ↑	PSNR ↑		QNR ↑
Brovey [1]	1.5730±0.0291	0.9341±0.0004	2.7190±0.2970	0.8929±0.0017	0.8600±0.0019	33.6284±2.3345		0.9353±0.0018
HPF [2]	1.7227±0.0668	0.9525±0.0001	3.1126±0.2483	0.8857±0.0010	0.8489±0.0011	32.8080±1.9174		0.9481±0.0008
LMVM [3]	1.7781±0.0941	0.9475±0.0002	2.5043±0.2554	0.9080±0.0014	0.8805±0.0016	34.9157±2.6255		0.9605±0.0002
PNN [4]	2.5468±0.0887	0.9246±0.0002	3.3448±0.1668	0.9010±0.0003	0.9020±0.0005	33.3837±2.1497		0.8652±0.0011
PanNet [6]	1.4493±0.0683	0.9633±0.0001	1.7392±0.1650	0.9581±0.0003	0.9465±0.0003	38.1128±4.0232		0.9545±0.0003
PSGAN [9]	2.1482±0.0530	0.9527±0.0000	2.1682±0.0808	0.9462±0.0001	0.9266±0.0002	36.4841±2.6874		0.9055±0.0007
PGMAN (W)	2.4217±0.0515	0.9166±0.0002	2.7940±0.1151	0.9030±0.0002	0.8683±0.0004	33.8740±2.0167		0.9344±0.0012
PGMAN (F)	2.2185±0.0346	0.9210±0.0002	2.6980±0.1270	0.9058±0.0002	0.8795±0.0004	34.2169±2.0992		0.9745±0.0001

TABLE III  
ABLATION RESULTS ON GAOFEN-2 IMAGES. ALL MODELS ARE TRAINED UNDER THE FULL-RESOLUTION SETTING.

$\mathcal{L}_{QNR}$	$\mathcal{L}_{adv}$	SAM ↓	sCC ↑	ERGAS ↓	Q4 ↑	SSIM ↑	PSNR ↑		QNR ↑
✓	✓	8.8467±2.9764	0.6833±0.0015	13.1840±6.5571	0.4647±0.0023	0.4863±0.0048	22.5740±1.5985		0.8116±0.0019
✓	✓	2.4422±0.0284	0.9240±0.0002	2.9252±0.0747	0.9267±0.0002	0.9026±0.0001	33.7254±0.5398		0.9865±0.0000
✓	✓	2.0763±0.0314	0.9342±0.0002	2.5761±0.0707	0.9385±0.0001	0.9151±0.0001	34.8360±0.7312		0.9874±0.0000

on GaoFen-2 and QuickBird images. This indicates that full-resolution images indeed provide rich spatial and spectral information which are helpful for improving the quality of the pan-sharpened images. When test ours and the comparison methods on full-scale images, our method shows significant advantages over all traditional and deep learning methods. It has the best QNR indicators on the two datasets and outperforms the comparison methods by a large margin, showing the great practical value of it. Even trained on down-sampled images, PGMAN(W) has a very good generalization ability to full-scale images.

#### D. Visual Results

Figs. 3 and 4 show some examples on GaoFen-2 and QuickBird images, respectively. Note that these results are produced from the original PAN and MS images. From Fig. 3 we can observe that traditional methods tend to distort colors. Brovey (Fig. 3(b)) presents obvious color distortion compared with the LR MS. HPF (Fig. 3(c)) and LMVM (Fig. 3(d)) blur the results. And deep learning based methods (Figs. 3(e)–(g)) also demonstrate low quality spatial details. Our method generate pan-sharpened images (Fig. 3(h) and (i)) with good spatial and color quality, especially when it was trained on the original PAN and MS images. Similar conclusions can be drawn from QuickBird full-scale testing results (Fig. 4).

#### E. Ablation Study

We conduct ablation studies to verify the effectiveness of the  $QNR$  loss on GaoFen-2 images. The results are shown in Table III, from which we can see that using only  $\mathcal{L}_{adv}$  produces poor results with unacceptable qualities. The  $QNR$  loss obtains promising results far better than adversarial loss in terms of all metrics. When combining these two losses together, the results can be further improved, especially on the reference-based indicators.

#### V. CONCLUSION

In this paper, we propose a novel unsupervised generative multi-adversarial model for pan-sharpening, called PGMAN. Under an unsupervised framework, our proposed method can be trained on either low-resolution or full-resolution images without ground truth. We focus on original PAN and LRMS images without any preprocessing step and achieve attractive performance on full-scale testing and satisfactory results on low-resolution images. In our future work, we will continue to study unsupervised models and further improve the performance.

#### REFERENCES

[1] A. R. Gillespie, A. B. Kahle, and R. E. Walker, "Color enhancement of highly correlated images. ii. channel ratio and "chromaticity" transfor-



(a) LR MS

(b) Brovey [1]

(c) HPF [2]



(d) LMVM [3]

(e) PNN [4]

(f) PanNet [6]



(g) PSGAN [9]

(h) PGMAN (W)

(i) PGMAN (F)

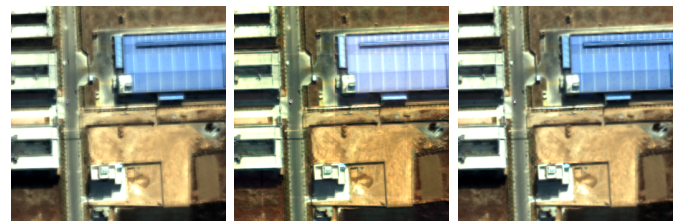
Fig. 3. Visual results on GaoFen-2 full-resolution images.



(a) LR MS

(b) Brovey [1]

(c) HPF [2]



(d) LMVM [3]

(e) PNN [4]

(f) PanNet [6]



(g) PSGAN [9]

(h) PGMAN (W)

(i) PGMAN (F)

Fig. 4. Visual results on QuickBird full-resolution dataset.

mation techniques,” *Remote Sensing of Environment*, vol. 22, no. 3, pp. 343–365, 1987.

[2] U. G. Gangkofner, P. S. Pradhan, and D. W. Holcomb, “Optimizing the high-pass filter addition technique for image fusion,” *Photogramm. Eng. Remote Sens.*, vol. 73, no. 9, pp. 1107–1118, 2007.

[3] S. de Béthune, F. Muller, and J.-P. Donnay, “Fusion of multispectral and panchromatic images by local mean and variance matching filtering techniques,” *Fusion of Earth Data*, pp. 28–30, 1998.

[4] G. Masi, D. Cozzolino, L. Verdoliva, and G. Scarpa, “Pansharpening by convolutional neural networks,” *Remote Sens.*, vol. 8, no. 7, p. 594, 2016.

[5] C. Dong, C. C. Loy, K. He, and X. Tang, “Image super-resolution using deep convolutional networks,” *IEEE Trans. Pattern anal. Mach. intellig.*, vol. 38, no. 2, pp. 295–307, 2015.

[6] J. Yang, X. Fu, Y. Hu, Y. Huang, X. Ding, and J. Paisley, “Pannet: A deep network architecture for pan-sharpening,” in *Proc. IEEE Int. Conf. Comput. Vis.*, 2017, pp. 5449–5457.

[7] K. He, X. Zhang, S. Ren, and J. Sun, “Deep residual learning for image recognition,” in *Proc. IEEE Conf. Comput. Vis. Pattern Recognit.*, 2016, pp. 770–778.

[8] X. Liu, Q. Liu, and Y. Wang, “Remote sensing image fusion based on two-stream fusion network,” *Inf. Fusion*, vol. 55, pp. 1–15, 2020.

[9] X. Liu, Y. Wang, and Q. Liu, “Psgan: a generative adversarial network for remote sensing image pan-sharpening,” in *IEEE Int. Conf. Image Process.* IEEE, 2018, pp. 873–877.

[10] I. Goodfellow, J. Pouget-Abadie, M. Mirza, B. Xu, D. Warde-Farley, S. Ozair, A. Courville, and Y. Bengio, “Generative adversarial nets,” in *Proc. Adv. Neural Inf. Proc. Syst.*, 2014, pp. 2672–2680.

[11] J.-Y. Zhu, T. Park, P. Isola, and A. A. Efros, “Unpaired image-to-image translation using cycle-consistent adversarial networks,” in *Proc. IEEE Int. Conf. Comput. Vis.*, 2017, pp. 2223–2232.

[12] L. Alparone, B. Aiazzi, S. Baronti, A. Garzelli, F. Nencini, and M. Selva, “Multispectral and panchromatic data fusion assessment without reference,” *Photogrammetric Engineering & Remote Sensing*, vol. 74, no. 2, pp. 193–200, 2008.

[13] M. Arjovsky, S. Chintala, and L. Bottou, “Wasserstein generative adversarial networks,” in *Int. Conf. Mach. Learn.*, 2017.

[14] I. Gulrajani, F. Ahmed, M. Arjovsky, V. Dumoulin, and A. C. Courville,

“Improved training of wasserstein gans,” in *Proc. Adv. Neural Inf. Process. Syst.*, 2017, pp. 5767–5777.

[15] I. Durugkar, I. Gemp, and S. Mahadevan, “Generative multi-adversarial networks,” in *Int. Conf. Learn. Represent.*, 2017.

[16] P. Isola, J.-Y. Zhu, T. Zhou, and A. A. Efros, “Image-to-image translation with conditional adversarial networks,” in *Proc. IEEE Conf. Comput. Vis. Pattern Recognit.*, 2017, pp. 1125–1134.

[17] L. Wald, T. Ranchin, and M. Mangolini, “Fusion of satellite images of different spatial resolutions: Assessing the quality of resulting images,” *Photogramm. Eng. remote Sens.*, vol. 63, no. 6, pp. 691–699, 1997.

[18] A. Paszke, S. Gross, F. Massa, A. Lerer, J. Bradbury, G. Chanan, T. Killeen, Z. Lin, N. Gimelshein, L. Antiga *et al.*, “Pytorch: An imperative style, high-performance deep learning library,” in *Proc. Adv. Neural Inf. Proc. Syst.*, 2019, pp. 8024–8035.

[19] D. P. Kingma and J. Ba, “Adam: A method for stochastic optimization,” *arXiv preprint arXiv:1412.6980*, 2014.

[20] R. H. Yuhas, A. F. Goetz, and J. W. Boardman, “Discrimination among semi-arid landscape endmembers using the spectral angle mapper (sam) algorithm,” in *JPL, Summaries of the Third Annual JPL Airborne Geoscience Workshop*, vol. Volume 1: AVIRIS Workshop, 1992.

[21] J. Zhou, D. Civco, and J. Silander, “A wavelet transform method to merge landsat tm and spot panchromatic data,” *International journal of remote sensing*, vol. 19, no. 4, pp. 743–757, 1998.

[22] L. Wald, “Quality of high resolution synthesised images: Is there a simple criterion?” in *Third Conference “Fusion of Earth data: merging point measurements, raster maps and remotely sensed images”*, 2000, pp. 99–103.

[23] Z. Wang and A. C. Bovik, “A universal image quality index,” *IEEE signal process. lett.*, vol. 9, no. 3, pp. 81–84, 2002.

[24] Z. Wang, A. C. Bovik, H. R. Sheikh, and E. P. Simoncelli, “Image quality assessment: from error visibility to structural similarity,” *IEEE Trans. Image process.*, vol. 13, no. 4, pp. 600–612, 2004.